Thermal Analysis of Wireless Power Transfer Coils for Dynamic Wireless Electric Vehicle Charging

Rafal Wojda
Electric Energy Systems Integration Group
Oak Ridge National Laboratory
Oak Ridge, TN 37830
Email: wojdarp@ornl.gov

Veda Prakash Galigekere
Power Electronics and Electric Machinery Group
Oak Ridge National Laboratory
Oak Ridge, TN 37830
Email: galigekerevn@ornl.gov

Jason Pries
Power Electronics and Electric Machinery Group
Oak Ridge National Laboratory
Oak Ridge, TN 37830
Email: priesjl@ornl.gov

Omer Onar
Power Electronics and Electric Machinery Group
Oak Ridge National Laboratory
Oak Ridge, TN 37830
Email: onaroc@ornl.gov

***Abstract*—In this paper, safe operating conditions of a wireless power transfer coil were identified and road infrastructure for a dynamic wireless electric vehicle charging system was studied. Magneto-thermal simulations were used to map the power loss directly into the computed fluid dynamics solver. This method allowed the authors to analyze the heating pattern of the enclosed wireless power transfer coil in the road structure, as well as for the vehicle coil. Thermal heating patterns for three types of rectangular coil structures were analyzed. Heating patterns were analyzed for 200 kW coils and different magnetic field densities in the magnetic core.**

I. Introduction

Extensive research is being performed in the field of electric vehicle wireless power transfer (WPT) and dynamic wireless power transfer [1]-[6]. High-power dynamic wireless charging is of increasing interest, with plans for 200 kW charging and beyond. Besides advantages such as high power, rapid charging, and maintenance-free charging, high-power WPT systems need to be studied in terms of the influence of the WPT coil on the road structure as well as the road structure on the primary coil. The typical asphalt road structure (Fig. 1 (a)) is composed of 40-75 mm high-quality asphalt at the top surface following into the ground with 100175 mm of a high-modulus material (HMM) layer, which is followed by 75-100 fatigue resistant material (FRM); HMM and FRM are usually intermediate layers, which are embedded at the pavement foundation up to 250 mm, called the base (in the simulations, the road depth is assumed to be 250 mm [7]-[10]). Most pavements in the United States are designed for a 50-year life cycle, including 20 years of resurfacing to improve friction and reduce noise and cracking. The design considers temperature, moisture, and ground water level [7], as well as tensile strains, aging, healing, and mixture composition.

This manuscript has been authored by UT-Battelle, LLC, under contract DE-AC05-00OR22725 with the US Department of Energy (DOE). The US government retains and the publisher, by accepting the article for publication, acknowledges that the US government retains a nonexclusive, paid-up, irrevocable, worldwide license to publish or reproduce the published form of this manuscript, or allow others to do so, for US government purposes. DOE will provide public access to these results of federally sponsored research in accordance with the DOE Public Access Plan (http://energy.gov/downloads/doe-public-access-plan).

Temperature is one significant factor analyzed in this study. Figure 1 shows the temperature gradient in the asphalt layers. Every layer is designed to operate within the maximum ambient temperature range. To assure stability and durability, surface and intermediate layers must be bound with a binder of high-temperature grading. This factor is crucial because high stresses induced by static and dynamic loads can otherwise cause rutting through shear failure. In this study three types of coils are investigated. First two coils are the primary coils that are embedded into the high-quality asphalt layer, where:

- Coil is partially buried (PB) in concrete asphalt with an exposed coil top surface (Fig. 1. (b)), and
- Coil is fully buried (FB), embedded into concrete asphalt (Fig. 1. (c)).

The third type of coil is a secondary coil in which core and winding are enclosed in epoxy glass housing and potted (enclosed and potted; EP) with thermally conductive silicone CoolTherm SC-320.

II. Coil Model Description

In this study, the coil enclosure was potted with CoolTherm, 200 kW (512 $\times$ 512 $\times$ 19.5 mm) square coil pairs, with N = 7 turns, litz wire copper winding with a cross-sectional area of 134.5365 mm^2 (equivalent to 2$\times$2 AWG), maximum root mean square (RMS) current I_{maxRMS} = 278 A, core thickness of 3.3 mm, polyamide wire insulation (Kapton), and epoxy glass enclosure. The self-inductances of the primary coil PB, primary coil FB, and secondary coils EP, and the mutual inductance at a 250 mm distance between coils were 30.17 μH, 30.17 μH, and 5.27 μH, respectively. The main assumption in the analysis was that the strand diameter was much smaller than the skin depth at 85 kHz, and therefore, no eddy current effects were in the wire [11]-[14]. This way, litz-wire winding could be modeled as a solid conductor and eddy current loss could be disregarded.

III. Boundary Conditions For Thermal Modeling Of The Road

To simulate the thermal heating pattern of the coil embedded into the concrete or asphalt road, the thermal conditions of

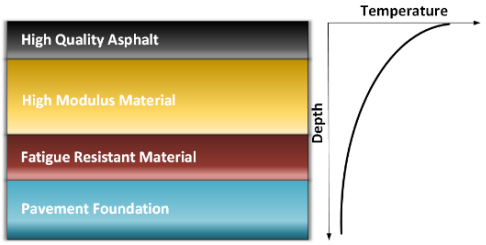

(a)

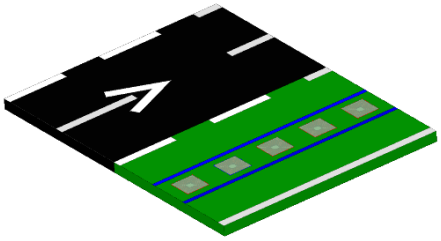

(b)

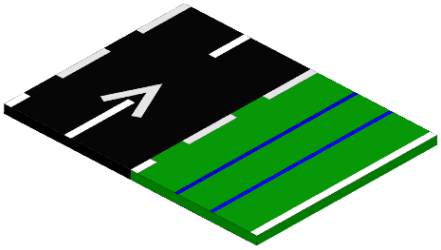

(c)

Fig. 1. Asphalt layers and temperature gradient in the concrete asphalt (a), coil PB in road surfacing material (b), and coil FB and embedded into road surfacing material (c).

the concrete-asphalt road had to be established. A model from Carmichael et al. [8] considers the mean air temperature T_M, its maximum variation T_V, depth below surface, bitumen conductivity, specific heat, density and diffusivity, and solar irradiation. In general, for semi-infinite soil mass, the pavement temperature is given by

$$T_p = T_M + T_V \sin(0.262t), \tag{1}$$

where t is time in hours. Figure 3 shows the surface temperature waveform for the asphalt road at T_M = 32°C. The figure shows that the maximum temperature of the road surface may reach up to 65°C. Therefore, the simulations were performed at the peak of surface temperature that may occur after 4 p.m. of the summer period. The model of the coil embedded into the ground is shown in Fig. 2(c). For estimation of the ground temperature, a method from the National Weather Service [15] was used. According to this model, the temperature of the soil is given by

$$T_{soil}(x) = T_a - T_{amb} \\ e^{\left(-x\sqrt{\frac{\pi}{356\alpha}}\right)} \cos\left(\frac{2\pi}{356}\left[d_{year} - d_{year|T_{min}} - \frac{x}{2}\sqrt{\frac{365}{\alpha\pi}}\right)\right), \tag{2}$$

where d_{year} is the day of the year, and $d_{year|Tmin}$ is the day of the year at which the minimum temperature is noted.

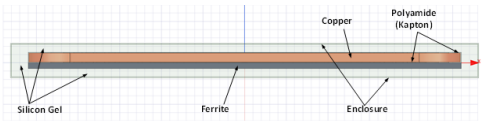

(a)

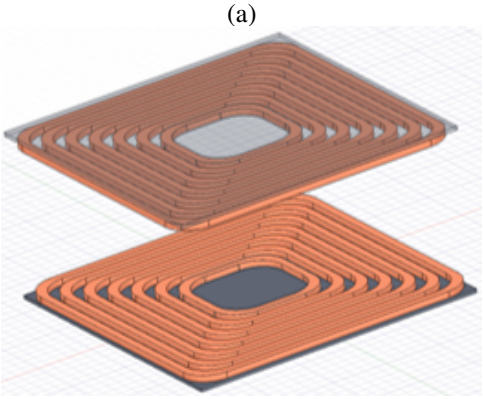

(b)

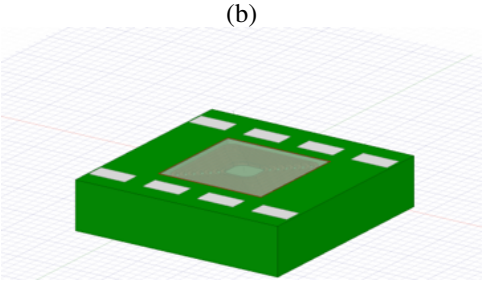

(c)

Fig. 2. Coil model. Coil components (a), 3D model of coupled coils (b), and model of the coil embedded into the ground (c).

TABLE I: THERMAL PARAMETERS FOR COMPUTATIONAL FLUID DYNAMICS SIMULATIONS

Material	κ	γ	c_p	ϵ
Copper	400	8,933	1.77e-5	0.052
3C95 Ferrite	4	4,800	1e-5	0.8
Polyamide	0.26	1,500	2.5e-5	0.82
Epoxy Glass	0.17	1,900	5e-5	0.93
Silicon Resin	3	700	0.00011	0.9
Asphalt Concrete	1.21	2,250	2.64e-5	0.93

Assuming the average temperature of T_a = 24.6°C, average high temperature of T_{amp} = 32.4°C (Miami, June 2018) [9], and diffusivity of the dry sand α = 0.001 (cm^2/s) [16], [17], the ground soil temperature is 31°C at x = 0.25 m under the surface (Fig. 3 (b)). The thermal parameters used for thermal simulations are given in Table I, where κ is thermal conductivity, γ is mass density (kg/m^3), C_p is specific heat (J·kg^{-1}·K^{-1}), and ϵ is surface emissivity.

IV. SIMULATIONS

Co-simulations of coils were performed using Ansys Maxwell 3D-Icpak solvers. The magnetic design was verified and simulated using eddy-current solver at f = 85 kHz and the power losses were mapped into the computational fluid dynamics Icepak solver. The initial condition for the

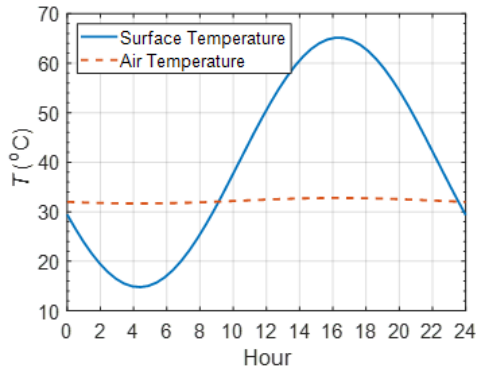

(a)

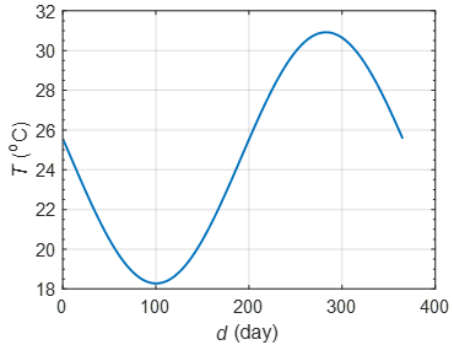

(b)

Fig. 3. Temperatures of ground and pavement. Daily pavement surface temperature at T_m = 32°C (a) and annual dry soil temperature variation at depth of 250 mm (b).

TABLE II: COMPUTATIONAL FLUID DYNAMICS THERMAL SIMULATION RESULTS

Coil elements		EP		PB		FB	
		Avg (°C)	Max (°C)	Avg (°C)	Max (°C)	Avg (°C)	Max (°C)
Turn 1	T_{ins}	119	119	165	165	186	186
	T_{wind}	119	119	163	163	183	183
Turn 2	T_{ins}	117	117	160	160	178	178
	T_{wind}	114	115	155	155	172	172
Turn 3	T_{ins}	110	110	148	148	163	164
	T_{wind}	103	104	139	140	152	154
Turn 4	T_{ins}	94	94	126	128	139	141
	T_{wind}	118	121	165	169	186	190
Turn 5	T_{ins}	118	121	163	167	182	187
	T_{wind}	117	120	159	164	178	183
Turn 6	T_{ins}	114	117	154	160	171	177
	T_{wind}	110	114	148	154	163	170
Turn 7	T_{ins}	103	108	138	145	152	160
	T_{wind}	93	99	126	134	138	148
Other	T_{core}	111	121	152	169	169	192
	$T_{silicone}$	103	121	141	169	157	192
	$T_{enclosure}$	99	117	135	168	150	190
	$T_{asphalt}$			82	166	88	188

TABLE III: CO-SIMULATIONS OF THE PB COIL AT DIFFERENT FLUX DENSITIES

B_{avg} (mT)	52	82	92	103	107	111	116	123	143	153	202
P_C (W)	17	52	69	90	100	110	120	140	200	240	506
$T_{ins(avg)}$ (°C)	62	71	76	82	84	87	89	94	108	117	170
$T_{ins(max)}$ (°C)	64	74	79	85	88	90	93	99	114	124	184
$T_{wind(avg)}$ (°C)	62	72	76	82	85	87	90	94	109	118	170
$T_{wind(max)}$ (°C)	64	74	79	84	87	90	92	98	113	123	180
$T_{core(avg)}$ (°C)	61	71	76	82	84	87	89	94	109	118	173
$T_{core(max)}$ (°C)	63	74	79	85	88	90	93	99	115	125	185
$T_{encl(avg)}$ (°C)	59	68	72	77	80	82	84	89	102	110	158
$T_{encl(max)}$ (°C)	63	73	78	84	87	90	93	98	114	124	184
$T_{silicone(avg)}$ (°C)	60	69	74	79	82	84	86	91	105	113	164
$T_{silicone(max)}$ (°C)	63	74	79	85	88	90	93	99	114	125	185
$T_{asphalt(avg)}$ (°C)	52	59	62	66	68	69	71	75	85	91	128
$T_{asphalt(max)}$ (°C)	65	73	78	84	86	89	92	97	113	123	182

simulations was I_{RMS} = 278 A, which resulted in an average flux density in the 3C95 ferrite core [17] B_{avg} = 263 mT. The simulated core loss was P_C = 965 W and the winding loss was P_w = 84 W for each coil (Fig. 2 (b)). For these power losses, the temperatures are shown in Table II for EP (secondary), PB (primary) and FB coils (primary), respectively. Table II shows that only EP coil can operate at B_{avg} = 263 mT because at this flux density, the maximum temperature is 121°C at the fifth turn insulation, as well as in the silicone and core. The maximum temperature of 121°C was assumed to be safe for the insulation (thermal class F), silicone, and core. However, for the primary coils (buried in the asphalt) the maximum temperatures were 169°C and more. For these coils, the asphalt hot-spot temperature was 166 and 188°C for PB and FB coils, respectively. Such temperatures are undesired for the road for three reasons. First, high temperature is not safe for the road user. Second, such a temperature of asphalt may cause rutting of the road causing reduction of the road life cycle. Third, high temperature of the road increases the temperature and pressure of the tire and causes further rutting. Therefore, to prevent the aforementioned problems, reduction of the coil loss is required. To reduce the coil loss significantly, the magnetic flux density must be reduced because the core losses depend on the flux density to the power 2.44 for the 3C95 core. The density loss for this core material is given by

$$P_c = 1.3056e^{7}B^{2.44}(4.262e^{-5}T^2 - 7.9389e^{-3}T + 1.3324T)\ \left(\frac{\mathrm{mW}}{cm^3}\right) \quad (3)$$

To reduce the flux density in the core, the thickness of the core had to be increased. Table IV shows the average temperature of the PB primary coil components as a functions of flux density. The increase of core thickness of the primary coil did not influence the mutual inductance. Table IV shows that for flux densities in the range of B_{avg} = 53 to 103 mT, the average temperature of the asphalt road is below 70°C, which is close to the surface temperature. The maximum temperatures are up to 84°C and are located just below the enclosure. For fluxes B_{avg} = 153 mT and higher, the average temperature of the asphalt road was around 91°C.

A. Conclusions

In this work, magneto-thermal co-simulations of 200 kW WPT coils were performed. The boundary conditions for

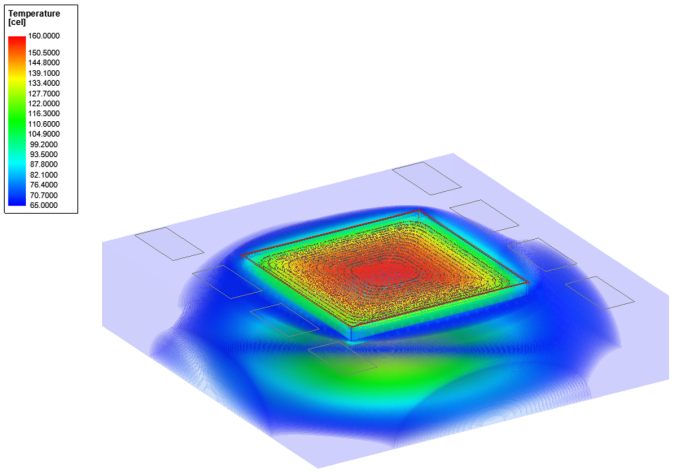

Fig. 4. Heat distribution in the WPT PB coil.

the thermal simulations were identified based on work from Charmichael et al. [8], [16]; the maximum road surface temperature and maximum ground temperature at depths of 0.25 m and below the road surface were used for simulations. For the EP coil made with 3C95 ferrite, the flux density of B_{avg} = 263 mT can be used for the receiver (secondary) coil because the temperatures of coil components are below the thermal class F threshold and no thermal runaway occur. Conversely, for the primary coils embedded in the road structure, such average flux density would cause overheating of the coil components, thermal runaway of the core, and melting of the road structure. To identify the safe flux densities of the 200 kW coil that has to be embedded into the road structure, thermal simulations of the PB coil were performed at different flux densities in the core (at different core thicknesses). Flux densities up to B_{avg} = 123 mT may be operated in PB coils without a significant influence on the road structure.

ACKNOWLEDGMENT

This research used resources at the Power Electronics and Electric Machinery Research Facility, a DOE Office of Science User Facility operated by the Oak Ridge National Laboratory.

REFERENCES

[1] J. Pries, V. P. Galigekere, O. C. Onar, G-J Su, R. Wiles, L. Seiber, J. Wilkins, S. Anwar, and S. Zou, "Coil Power Density Optimization and Trade-off Study for a 100kW Electric Vehicle IPT Wireless Charging System," 2018 IEEE Energy Conversion Congress and Exposition (ECCE), Sept. 2327, Portland, Oregon, USA, 2018.

[2] Q. Deng, J. Liu, D. Czarkowski, M. K. Kazimierczuk, M. Bojarski, H. Zhou, and W. Hu, "Frequency-Dependent Resistance of Litz-Wire Square Solenoid Coils and Quality Factor Optimization for Wireless Power Transfer," *IEEE Transactions on Industrial Electronics*, vol. 63, no. 5, May 2016.

[3] D. Howel, et al., Enabling Fast Charging: A Technology Gap Assessment. US Department of Energy, Oct. 2017.

[4] "Wireless charging for electric vehicles," Momentum Dynamics, https://www.momentumdynamics.com/.

[5] "Technology," ELIX Wireless, https://www.elixwireless.com/technology.

[6] Sargand, S .M., I. S. Khoury, M. T. Romanello, and J. L. Figueroa, "Seasonal and Load Response Instrumentation of the Way-30 Perpetual Pavement." Proc. of the International Conference on Perpetual Pavements. Ohio University, Columbus, Ohio, USA, 2006.

[7] E. S. Barber, "Calculation of Maximum Pavement Temperatures From Weather Reports," Highway Research Board Bulletin 168, National Research Council, Washington, D.C., 1957, pp. 18.

[8] T. Carmichael, R. E. Boyer, and L. D. Hokanson, "Modeling Heater Techniques for In-Place Recycling of Asphalt Pavements," Proc. Association of Asphalt Paving Technologists, Vol. 46, 1977, pp. 526540.

[9] Kasuda, T., and P. R. Archenbach, "Earth Temperature and Thermal Diffusivity at Selected Stations in the United States," *ASHRAE Tran.*, vol. 71, Part 1, 1965.

[10] "CoolTherm SC-320 THK Thermally Conductive Silicone," Parker, https://www.lord.com/products-and-solutions/electronic-materials/cooltherm-sc-320-THK-thermally-conductive-silicone.

[11] R.P. Wojda and M. K. Kazimierczuk, "Winding Resistance of Litz-wire and Multi-strand Inductors," em IET Pow. Electron., vol. 5, no. 2, 2012.

[12] R.P. Wojda and M. K. Kazimierczuk, "Winding Resistance and Power Loss of Inductors With Litz and Solid-round Wires," *IEEE Ind. Applications.*, vol. 54, no. 4, 2018.

[13] J. Acero, P. J. Hernandez, J. M. Burdio, R. Alonso and L. A. Barragdan, "Simple Resistance Calculation in Litz-wire Planar Windings for Induction Cooking Appliances," *IEEE Tran. on Magnetics*, vol. 41, no. 4, pp. 12801288, April 2005.

[14] M. Czerwienko, A. Uramek, and R. P. Wojda, "Derivation of The Planar Square Coil Litz-wire Winding Resistance for Sinusoidal Currents," Przeglad Elektrotechniczny, vol. 6, 2019.

[15] "NWS Forecast Office Miami - South Florida," National Weather Service, https://www.weather.gov/mfl/.

[16] T. Carmichael, R. E. Boyer, and L. D. Hokanson, "Modeling Heater Techniques for In-Place Recycling of Asphalt Pavements," Proceedings of the Association of Asphalt Paving Technologists, Vol. 46, pp. 526540, 1977.

[17] "Power Conversion," Ferroxcube, https://ferroxcube.com.en-global/ak_material/index/power_conversion